Journal of Alloys and Compounds 511 (2012) 144–148

Contents lists available at SciVerse ScienceDirect

Journal of Alloys and Compounds

journal homepage: www.elsevier.com/locate/jallcom

Structural and electrical properties of $Gd(Ni_{1/2}Zr_{1/2})O_3$

Nishant Kumar [b], Alo Dutta [a,*], S. Prasad [b], T.P. Sinha [a]

[a] Department of Physics, Bose Institute, 93/1, Acharya Prafulla Chandra Road, Kolkata 700009, India
[b] Department of Physics, T.M. Bhagalpur University, Bhagalpur 812007, India

ARTICLE INFO

Article history:
Received 10 March 2011
Received in revised form 1 September 2011
Accepted 2 September 2011
Available online 10 September 2011

Keywords:
$Gd(Ni_{1/2}Zr_{1/2})O_3$
Impedance spectroscopy
Dielectric relaxation

ABSTRACT

The $Gd(Ni_{1/2}Zr_{1/2})O_3$ (GNZ) ceramic is synthesized by the solid-state reaction technique. The X-ray diffraction pattern of the sample shows monoclinic phase at room temperature. The dielectric dispersion of the material is investigated in the temperature range from 303 K to 673 K and in the frequency range from 100 Hz to 1 MHz. The relaxation peak is observed in the frequency dependence of the loss tangent. The relaxation time at different temperatures is found to obey Arrhenius law having activation energy of 1.1 eV which indicates the hopping of ions at the lattice site and may be responsible for the dielectric relaxation of GNZ. The scaling behaviour of loss tangent suggests that the relaxation mechanism is temperature independent. The frequency dependent conductivity spectra follow the power law. In the impedance formalism, the Cole–Cole model is used to study the relaxation mechanism of GNZ.

1. Introduction

The structural and transport properties of the perovskite oxide (ABO_3) in the category of the strongly correlated electron system containing transition metal at the B-site have been widely investigated because these characteristics are directly related to the localized d-electrons of transition metal ion. The perovskite oxides having chemical formula RMO_3 (R = rare earth element, M = 3d transition metal) have attracted the scientific interest to investigate the substitutional effect of various elements at the R and M sites [1–4]. Among them, rare earth nickelates ($RNiO_3$) are extensively studied from the technological point of view due to its unusual electronic and magnetic properties [5–8]. An insulator to metal transition is observed in $RNiO_3$ at a particular temperature. The transition temperature is found to increase when R is substituted by lanthanide ion of smaller radius. From the structural point of view, the $RNiO_3$ compounds are orthorhombically distorted perovskites. The unit cell distortion as well as the Ni–O–Ni bond angle is related to the rare-earth ionic size. The distortion of the NiO_6 octahedra increases if the rare earth ionic size decreases. This increase in NiO_6 distortion may be a consequence of higher electro-negativity of smaller rare earth ions.

In a recent study Kim et al. [9] have investigated the frequency dependent dielectric behaviour of gadolinium nickel titanate $Gd(Ni_{1/2}Ti_{1/2})O_3$ as function of temperature. This has motivated us to study the dielectric properties of a similar system gadolinium nickel zirconate $Gd(Ni_{1/2}Zr_{1/2})O_3$ (GNZ) when Ti is substituted by Zr, a member of the same column of periodic table. In a previous study we have also investigated the dielectric properties of a lanthanide based nickelate, samarium nickel zirconate, $Sm(Ni_{1/2}Zr_{1/2})O_3$ (SNZ) [10] by alternating current impedance spectroscopy (ACIS). ACIS is a very convenient and powerful experimental tool to investigate the contribution of various electroactive regions to the relaxation process of perovskite oxides [11,12]. This method describes the electrical processes occurring in a system on applying an ac signal as an input perturbation. This technique has been applied to analyze the relaxation spectrum of many bulk materials [13–17].

2. Experimental

The ceramic method was employed for the synthesis of GNZ. Reagent grade powders of Gd_2O_3 (Sigma–Aldrich), $NiCO_3$ (Loba Chemie) and ZrO_2 (Loba Chemie) having purity of more than 99% were taken in stoichiometric ratio and mixed in the presence of acetone for 12 h. The mixture was calcined at 1350 °C in air for 12 h and brought to room temperature at a cooling rate of 100 °C/h. The calcined sample was palletized into a disc using polyvinyl alcohol as binder. Finally, the discs were sintered at 1370 °C for 4 h and cooled down to room temperature at the cooling rate of 60 °C/h. The density of the sintered pellet measured by Archimedes' principle was found to be 5.36 g/cc, which indicated the densification of the pellet.

The X-ray diffraction (XRD) pattern of the sample was taken at room temperature using an automatic X-ray powder diffractometer (Rigaku Miniflex-II). The microstructure of the sample was observed by scanning electron microscope (SEM) (FEI Quanta 200). Fourier transform infrared (FT-IR) spectrum was recorded

* Corresponding author. Tel.: +91 33 23031189; fax: +91 33 23506790.
E-mail address: alo.dutta@yahoo.com (A. Dutta).

0925-8388/$ – see front matter © 2011 Elsevier B.V. All rights reserved.
doi:10.1016/j.jallcom.2011.09.011

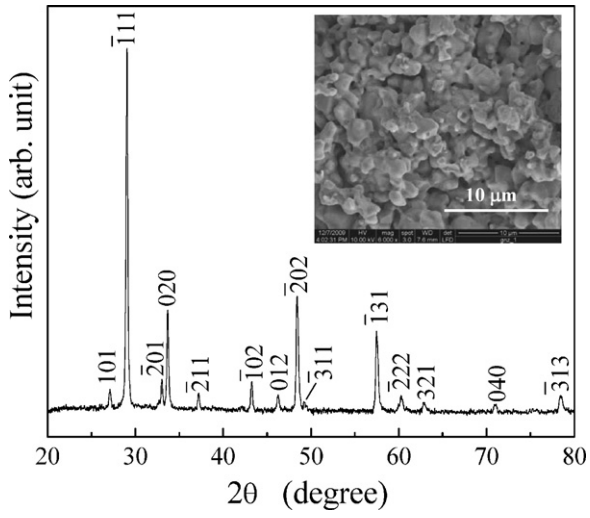

Fig. 1. XRD pattern of $Gd(Ni_{1/2}Zr_{1/2})O_3$ at room temperature. Scanning electron micrograph is shown in the inset.

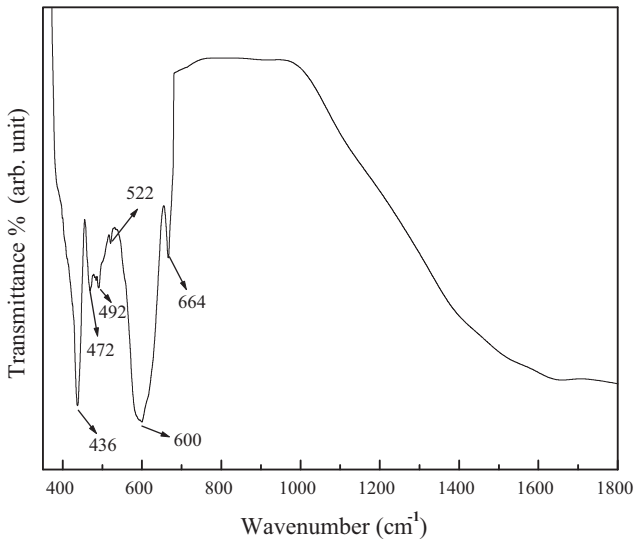

Fig. 2. FTIR spectrum of $Gd(Ni_{1/2}Zr_{1/2})O_3$.

in the transmittance mode at room temperature between 350 and 2000 cm^{-1} with an FT-IR spectrometer (Perkin Elmer Spectrum 1000) using the KBr pellet technique. For the dielectric characterization, the sintered disc (of thickness 1.49 mm and diameter 9.86 mm) was polished, electroded with fine silver paint and then connected to the LCR meter (Hioki). The capacitance, loss tangent and impedance of the sample were measured in the frequency range from 100 Hz to 1 MHz and in the temperature range from 303 K to 673 K. The temperature was controlled with a programmable oven. All the dielectric data were collected while heating at a rate of 0.5 °C min^{-1}. Each measured temperature was kept constant with an accuracy of ± 1 °C.

3. Results and discussion

3.1. Structural study

Fig. 1 shows the XRD pattern of the sample at room temperature. All the reflection peaks of the X-ray profile are indexed, and the interplaner spacings (d-values) and lattice parameters are determined using a least-squares method with the help of a standard computer programme (Crysfire). Good agreement between the observed and calculated interplaner spacings and no trace of any unaccounted peak in the diffraction pattern suggest the formation of a single-phase compound having monoclinic structure with $a = 6.34$ Å, $b = 5.31$ Å, $c = 4.26$ Å and $\beta = 98.07°$. If compared with the structure of SNZ [10] (where $a = 11.39$ Å, $b = 5.34$ Å, $c = 3.37$ Å and $\beta = 96°$), the unit cell volume of GNZ is found to be smaller than SNZ. This is due to the smaller ionic radius of Gd^{3+} (1.2 Å) in comparison to Sm^{3+} (1.24 Å). A higher value of angle β for GNZ indicates more distortion of the NiO_6 octahedra in GNZ with respect to SNZ. The SEM micrograph indicates the granular characteristic of GNZ as shown in the inset of Fig. 1. The average grain size of the specimen is found to be ~2 μm.

In simple ABO_3 perovskite with ideal cubic structure, three infrared active modes are observed in the first order vibrational spectrum. As the symmetry of the crystal structure deviates from the ideal cubic structure, the FTIR spectrum of complex perovskite, $A(B'_{1/2}B''_{1/2})O_3$ (1:1 order) contains more vibrational bands. This is because the introduction of two different atoms or elements of unlike valences at the B sites promotes the loss of both translational and inversion symmetries and, consequently, additional modes of vibration will appear in the FTIR spectrum. Fig. 2 shows the FT-IR spectrum of GNZ. All the peaks in the spectrum are the characteristic of the material. The lower energy band found in between 436 cm^{-1} and 522 cm^{-1} is related to the deformational (banding) mode of the BO_6 polyhedra. The energy band found in between 600 cm^{-1} and 664 cm^{-1} is due to the asymmetric BO_6 stretching vibration arising from the higher charge of the cation. The large width of the band at 600 cm^{-1} may be due to the overlapping of the ZrO_6 and NiO_6 vibrational modes [18–21].

3.2. Dielectric study

The angular frequency ω (=$2\pi\nu$) dependence of the dielectric constant, ε' and the loss tangent, tan δ for GNZ is plotted in Fig. 3 as a function of temperature. It is observed from Fig. 3(a) that the value of ε' decreases with increasing frequency which can be explained from the Debye theory [22]. At very low frequencies ($\omega \ll 1/\tau$, where τ is the relaxation time), dipoles follow the field and we have $\varepsilon' \approx \varepsilon_s$ (value of the dielectric constant at quasi-static fields). With the increase of frequency (when $\omega < 1/\tau$), dipoles begin to lag behind the field and ε' slightly decreases. When frequency reaches the characteristic frequency ($\omega = 1/\tau$), the dielectric constant drops (relaxation process). At very high frequencies ($\omega \gg 1/\tau$), dipoles can no longer follow the field and $\varepsilon' \approx \varepsilon_\infty$ (high frequency value of ε'). Since our frequency window of measurement starts from 100 Hz, the first two parts are not observed in Fig. 3(a). The sharp increase of ε' above 573 K at frequencies lower than 1 KHz may be attributed to the space charge polarization at the grain-boundary or at the specimen–electrode interface. The relaxation peak is developed in the angular frequency dependence of loss tangent at the dispersion region of ε' as shown in Fig. 3(b). The peak position in tan δ shifts to higher frequency side with increasing temperature. When the temperature is high, the rate of polarization formed is quick, and thus the relaxation occurs in high frequency. For the measurement of the characteristic relaxation time (τ_m), one can choose the inverse of frequency of the peak position in tan δ versus log ω plots in Fig. 3(b), i.e., $\tau_m = \omega_m{}^{-1}$. The temperature dependence of the characteristic relaxation time is shown in the inset of Fig. 3(a), which satisfies the Arrhenius law given by

$$\omega_m = \omega_0 \exp\left[-\frac{E_a}{K_B T}\right] \quad (1)$$

where ω_m is the angular frequency corresponding to peak maximum, ω_0 is the pre exponential factor, E_a is the activation energy required for dielectric relaxation, T is the measuring temperature and K_B is the Boltzmann constant. From the numerical fitting

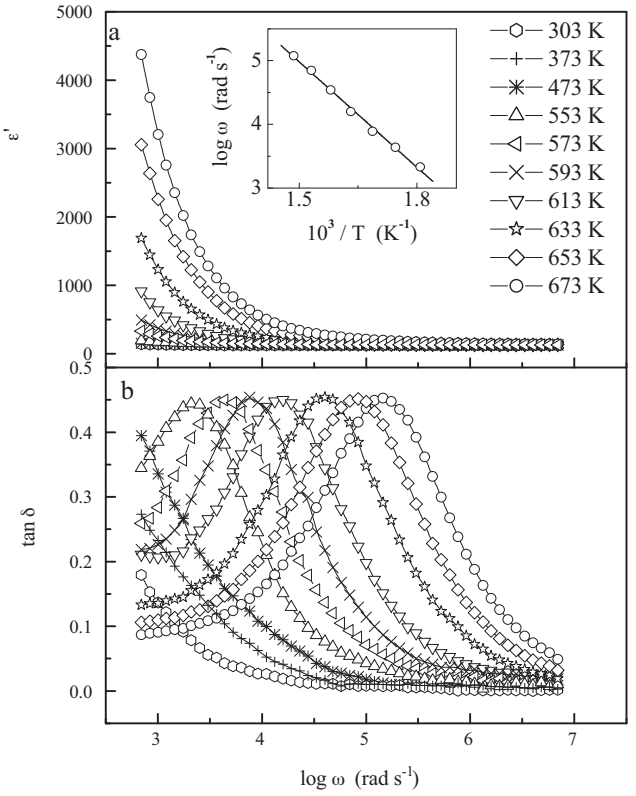

Fig. 3. Frequency (angular) dependence of ε' (a) and tan δ (b) at various temperatures for $Gd(Ni_{1/2}Zr_{1/2})O_3$. Arrhenius plot of most probable relaxation frequency is shown in the inset of (a) where the symbols are the experimental data points and the solid line is the least-squares straight-line fit.

analysis, we have obtained the value of the activation energy = 1.1 eV and τ_0 $(=1/\omega_0) = 1.1 \times 10^{-13}$ s. Such values of activation energy and pre exponential factor suggest that the relaxation phenomenon in GNZ is due to the hopping of ions at the lattice sites.

We have scaled each tan δ by tan δ_m (tan δ_m is the peak value of loss tangent) and each frequency by ω_m in Fig. 4. The overlap of the curves into a single master curve for all the temperatures indicates that the relaxation describes the same mechanism at different temperatures.

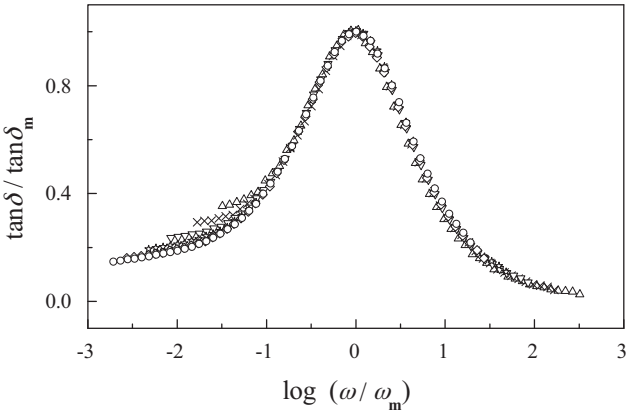

Fig. 4. Scaling behaviour of tan δ for $Gd(Ni_{1/2}Zr_{1/2})O_3$.

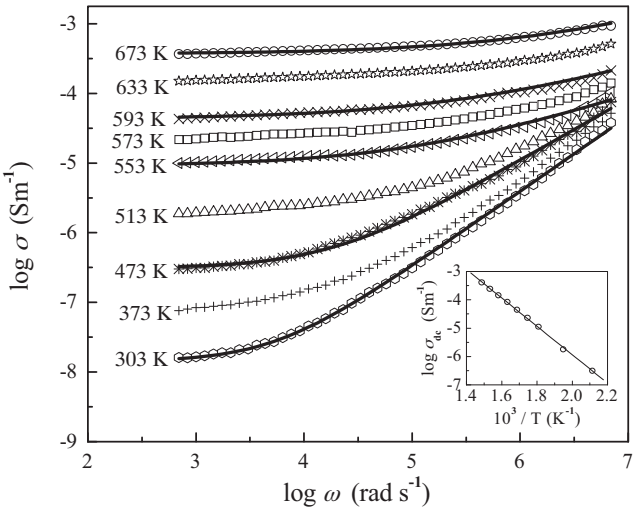

Fig. 5. Frequency (angular) dependence of the ac conductivity (σ) of $Gd(Ni_{1/2}Zr_{1/2})O_3$ at various temperatures where the symbols are the experimental points and the solid lines represent the fitting to Eq. (2). Temperature dependence of dc conductivity is shown in the inset where the symbols are the experimental points and the solid line is the least-squares straight-line fit.

3.3. Conductivity study

If one assumes that the total dielectric loss in the temperature range studied is due to conductivity, the appropriate formula for conductivity is $\sigma = \omega\varepsilon_0\varepsilon'\tan\delta$, here σ is the real part of the conductivity. The frequency dependent conductivity spectra of GNZ at different measuring temperatures are shown in Fig. 5. The conductivity shows dispersion which shifts to higher frequency side with the increase of temperature. It is observed from the Fig. 5 that σ decreases with decreasing frequency and becomes independent of frequency after a certain value giving σ_{dc}. The conductivity spectra follow the Jonscher power law [23] defined as

$$\sigma = \sigma_{dc}\left[1 + \left(\frac{\omega}{\omega_H}\right)^n\right] \quad (2)$$

where σ_{dc} is the dc conductivity, ω_H is the hopping frequency of the charge carriers, and n is the dimensionless frequency exponent. The experimental conductivity spectra of GNZ are fitted to Eq. (2) with σ_{dc} and ω_H as variables keeping in mind that the values of parameter n are weakly temperature dependent. The value of n is fixed at a particular temperature. The solid lines in Fig. 5 are the fitting of the experimental data with Eq. (2). The values of n obtained from the best fitting are found to be 0.45, 0.46, 0.51, 0.89 and 0.97 at 673, 593, 553, 473 and 303 K respectively.

The very basic fact about AC conductivity in GNZ is that σ is an increasing function of frequency (any hopping model has this feature). In a hopping model it is possible to distinguish different characteristic regions of frequency. At low frequencies where the conductivity is constant, the transport takes place on infinite paths. For a region of frequencies where the conductivity increases strongly with frequency, the carriers can hop only between two sites and a total response is produced by the sum of the individual response of pairs of sites randomly distributed throughout the material.

The temperature dependence of σ_{dc} as shown in the inset of Fig. 5 follows the Arrhenius law with an activation energy of 1 eV. The nearly same activation energy for dc conductivity and dielectric relaxation as obtained from the temperature dependence of most probable relaxation time for tan δ indicates that the same charge carriers are responsible for dielectric relaxation and conductivity in GNZ.

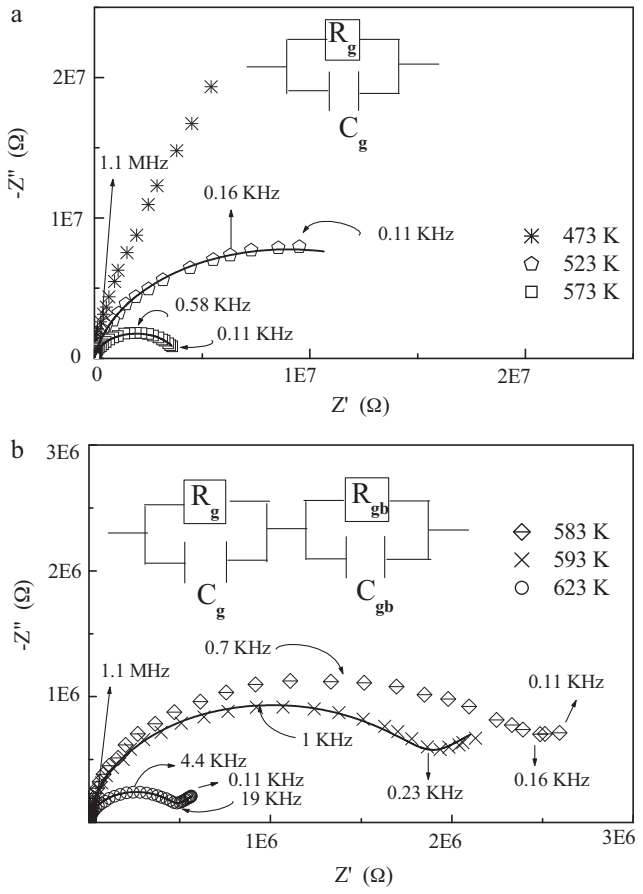

Fig. 6. Nyquist plots for $Gd(Ni_{1/2}Zr_{1/2})O_3$ at various temperatures. Solid lines are the fitting to Eq. (4).

3.4. Complex impedance study

We have also adopted the impedance formalism to study the relaxation mechanism in GNZ. The Nyquist plots (i.e., Z' vs. Z'' plots) are shown in Fig. 6 at various temperatures. In the impedance formalism, one can separate the different contributions arising from grain, grain-boundary and specimen–electrode interface in the relaxation process. Each of these contributions gives rise to a circular/semicircular arc in the Nyquist plot where higher frequency arc corresponds to the grain effect, mid-frequency arc is attributed to the grain-boundary effect and lower frequency arc represents the electrode effect. It is observed from Fig. 6(a) that up to 573 K only one semi-circular arc is observed which indicates the grain effect in relaxation phenomenon. When the temperature increases above 573 K the second semi-circular arc in the lower frequency side starts appearing due to the grain-boundary effect and its contribution increases with increasing temperature as shown in Fig. 6(b). The effect of grain and grain-boundary contributions in the material can be separated by fitting the experimental response to that of an electrical equivalent circuit, which is usually considered to comprise a series of parallel resistor–capacitor (R–C) elements. If the circuit consists of a series array of two sub-circuits of parallel R–C elements, one representing the grain effect and the other grain boundary, the complex impedance can be defined as:

$$Z^* = \frac{1}{R_g^{-1} + j\omega C_g} + \frac{1}{R_{gb}^{-1} + j\omega C_{gb}} \quad (3)$$

where R_g, R_{gb} and C_g, C_{gb} are the resistances and capacitances of grain and grain-boundary respectively. Based on Eq. (3), the response peaks of the grain and grain-boundary arcs are positioned at $1/(2\pi R_g C_g)$ and $1/(2\pi R_{gb} C_{gb})$, respectively, and the peak values are proportional to the associated resistances. In general, the peak frequency of grain-boundary is much lower than that for grain due to its large resistance and capacitance in comparison to grain [24].

Table 1
Fitting parameters of Nyquist plots obtained using Eq. (4).

Temperature (K)	ρ_g (Ω)	ε'_g	ρ_{gb} (Ω/m)	ε'_{gb}	α
523 K	1.02×10^6	76.43	–	–	0.42
573 K	2.20×10^5	79.3	–	–	0.4
593 K	1.07×10^5	81.5	1.13×10^5	1.3×10^4	0.39
623 K	2.77×10^4	93.6	5.1×10^4	3.3×10^4	0.388

Due to the depressed nature of the semicircular arcs of Nyquist plots as seen in Fig. 6, the experimental data cannot be well described by the Eq. (3). However, we find that the complex plane plot is better described by the Cole–Cole equation [25,26] which is commonly used for polycrystalline ceramic samples [27] and which modifies the Eq. (3) as follows:

$$Z^* = \frac{R_g}{1 + (j\omega\tau_g)^{1-\alpha}} + \frac{R_{gb}}{1 + (j\omega\tau_{gb})^{1-\alpha}} \quad (4)$$

where $\tau_g = R_g C_g$, $\tau_{gb} = R_{gb} C_{gb}$ and the parameter α is constant ($0 < \alpha \leq 1$). The solid lines in Fig. 6 show the fitting of the experimental data using Eq. (4). The fitted parameters at different temperatures are listed in Table 1 in terms of permittivity and resistivity of the materials. As shown in Fig. 6(a), the Nyquist plot is fitted to a single $R_g C_g$ parallel circuit due to the presence of only one semicircular arc in the high frequency region.

Going further to the description of experimental data for GNZ, the variation of the normalized parameters, tan δ/tan δ_m and Z''/Z''_m measured at 653 K as a function of logarithmic frequency for GNZ is shown in Fig. 7. A comparison of the loss tangent with impedance data allows one to determine the localized (i.e., defect) relaxation or non-localized conduction (i.e., ionic or electronic conductivity) in the dielectric materials [28]. It is possible to determine the type of the dielectric response by inspection of the magnitude of overlapping between the peaks of both the parameters tan δ (ω) and Z'' (ω). The overlapping peak position of tan δ/tan δ_m and Z''/Z''_m curves is an evidence of delocalized or long-range relaxation [28]. It is observed from Fig. 7 that for the present system the tan δ/tan δ_m and Z''/Z''_m peaks do not overlap but are close suggesting the components from both long-range and localized relaxations.

When compared with SNZ [10], it is observed that the values of dielectric constant and conductivity for GNZ are less than SNZ. This

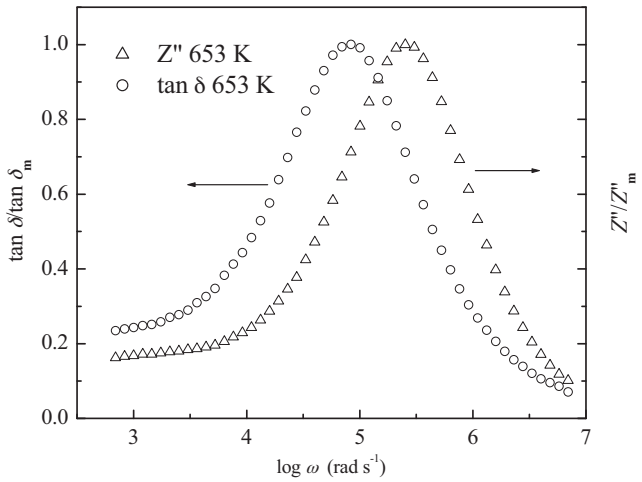

Fig. 7. Frequency dependence of tan δ/tan δ_m and Z''/Z''_m for $Gd(Ni_{1/2}Zr_{1/2})O_3$ at 653 K.

is because when the distortion in NiO_6 octahedra increases as one moves from Sm to Gd, the Ni–O–Ni bond angle decreases. Therefore, the hybridization between oxygen 2p-states and Ni-3d states is weakened resulting in a decrease in conductivity, and hence a decrease in the value of ε' for GNZ.

4. Conclusions

The dielectric relaxation of GNZ ceramic synthesized by the solid-state reaction technique is investigated in the temperature range from 303 K to 673 K and in the frequency range from 100 Hz to 1 MHz. The X-ray diffraction of the sample shows monoclinic structure at room temperature. The temperature dependent relaxation times are found to obey Arrhenius law having activation energy of 1 eV which indicates that the hopping of ions at the lattice site is responsible for conduction or dielectric relaxation in GNZ. The Nyquist plots show that above 573 K the grain-boundary effect appears along with the grain effect. The experimental data are well fitted with the Cole–Cole model. The frequency dependent conductivity spectra follow the power law. The scaling behaviour of tan δ suggests that the relaxation mechanism in GNZ is temperature independent. The non-overlapping peaks of frequency dependent tan δ/tan δ_m and Z''/Z''_m correspond to both long-range and localized relaxations.

Acknowledgement

This work is financially supported by Department of Science and Technology of India under grant no. SR/S2/CMP-01/2008.

References

[1] G. Giovannetti, S. Kumar, D. Khomskii, S. Picozzi, J. van den Brink, Phys. Rev. Lett. 103 (2009), 156401-1-4.
[2] I.I. Mazin, D.I. Khomskii, R. Lengsdorf, J.A. Alonso, W.G. Marshall, R.M. Ibberson, A. Podlesnyak, M.J. Martinez-Lope, M.M. Abd-Elmeguid, Phys. Rev. Lett. 98 (2007) 176406-1-4.
[3] M. Kriener, C. Zobel, A. Reichl, K. Baier, M. Cwik, K. Beggold, H. Kierspel, O. Zabara, A. Freimuth, T. Lorenz, Phys. Rev. B 69 (2004) 094417-1-7.
[4] J.-Q. Yan, J.-S. Ahou, J.B. Goodenough, Phys. Rev. B 69 (2004), 134409-1-6.
[5] Mridula Biswas, J. Alloys Compd. 480 (2009) 942–946.
[6] Y. Bodenthin, U. Staub, C. Piamonteze, M. Garcĩıa-Fernĩandez, M.J. Martĩınez-Lope, J.A. Alonso, J. Phys.: Condens. Mater. 23 (2011), 036002-1-8.
[7] V.B. Barbeta, R.F. Jardim, M.S. Torikachvili, M.T. Escote, F. Cordero, F.M. Pontes, F. Trequattrini, J. Appl. Phys. 109 (2011), 07E115-1-3.
[8] J.-G. Cheng, J.-S. Zhou, J.B. Goodenough, J.A. Alonso, M.J. Martinez-Lope, Phys. Rev. B 82 (2010), 085107-1-7.
[9] D.J. Kim, S. Park, M.S. Jang, I.-K. Jeong, C.H. Park, S.S. Park, J.S. Bae, J.P. Kim, K.S. Hong, E.D. Jeong, Y.S. Kim, J. Korean Phys. Soc. 53 (2008) 3371–3374.
[10] Nishant Kumar, Alo Datta, S. Prasad, T.P. Sinha, Phys. B 405 (2010) 4413–4417.
[11] W. Chena, W. Zhua, C. Kea, Z. Yanga, L. Wangb, X.F. Chena, O.K. Tana, J. Alloys Compd. 508 (2010) 141–146.
[12] R. Ranjan, R. Kumar, N. Kumar, B. Behera, R.N.P. Choudhary, J. Alloys Compd. 509 (2011) 6388–6394.
[13] Alo Dutta, T.P. Sinha, Phys. B 405 (2010) 1475–1479.
[14] Alo Dutta, T.P. Sinha, J. Alloys Compd. 509 (2011) 1705–1710.
[15] Moti Ram, J. Alloys Compd. 509 (2011) 1744–1748.
[16] N.V. Minh, N.G. Quana, J. Alloys Compd. 509 (2011) 2663–2666.
[17] X-Zhong Xionga, Z-Guo Liua, J-Hu Ouyang, X-Liang Xiaa, J. Xianga, X-Ming Liua, J. Alloys Compd. 509 (2011) 8392–8397.
[18] M. Enhessari, S. Khanahmadzadeh, K. Ozaee, J. Iran. Chem. Res. 3 (2010) 11–15.
[19] H.P. Kumar, C. Vijayakumar, C.N. George, S. Solomon, R. Jose, J.K. Thomas, J. Koshy, J. Alloys Compd. 458 (2008) 528–531.
[20] R. Gottschall, R. Schöllhorn, M. Muhler, N. Jansen, D. Walcher, P. Gütlich, Inorg. Chem. 37 (1998) 1513–1518.
[21] J.D.G. Fernandes, D.M.A. Melo, L.B. Zinner, C.M. Salustiano, Z.R. Silva, A.E. Martinelli, M. Cerqueira, C. Alves Júnior, E. Longo, M.I.B. Bernardi, Mater. Lett. 53 (2002) 122–125.
[22] P. Debye, Polar Molecules, Chemical Catalogue Company, New York, 1929.
[23] A.K. Jonscher, Universal Relaxation Law, Chelsea Dielectrics Press, London, 1996.
[24] D.C. Sinclair, T.B. Adams, F.D. Morrison, A.R. West, Appl. Phys. Lett. 80 (2002) 2153–2155.
[25] K.S. Cole, R.H. Cole, J. Chem. Phys. 9 (1941) 342–351.
[26] J.R. Macdonald, Impedance Spectroscopy, Wiley, New York, 2005.
[27] J. Liu, C. Duan, W.N. Mei, R.W. Smith, J.R. Hardy, J. Appl. Phys. 98 (2005), 093703-1-5.
[28] R. Gerhardt, J. Phys. Chem. Solids 55 (1994) 1491–1506.